RESEARCH ARTICLE | DECEMBER 05 2016

Efficiency of four-wave mixing in injection-locked InAs/GaAs quantum-dot lasers

H. Huang; D. Arsenijević ; K. Schires; T. Sadeev; D. Erasme; D. Bimberg; F. Grillot

AIP Advances 6, 125105 (2016)
https://doi.org/10.1063/1.4971271

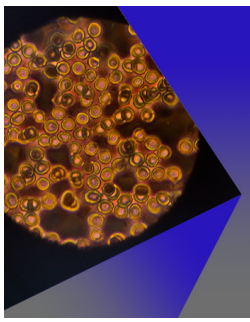

Efficiency of four-wave mixing in injection-locked InAs/GaAs quantum-dot lasers

H. Huang,[1,a] D. Arsenijević,[2] K. Schires,[1] T. Sadeev,[2] D. Erasme,[1] D. Bimberg,[2,b] and F. Grillot[1,c]
[1]*CNRS LTCI, Télécom ParisTech, Université Paris-Saclay, 46 rue Barrault, 75013 Paris, France*
[2]*Institut für Festkörperphysik, Technische Universität Berlin, Berlin 10623, Germany*

(Received 27 July 2016; accepted 17 November 2016; published online 5 December 2016)

Frequency conversion using highly non-degenerate four-wave mixing is investigated in optically injection-locked InAs/GaAs quantum-dot Fabry-Perot lasers with different ridge waveguide dimensions. Conversion efficiencies up to -16 dB with a large optical signal-to-noise ratios of 36 dB are unveiled. The conversion bandwidth is extended to 4 THz with a quasi-symmetrical response between up- and down-converted signals. [http://dx.doi.org/10.1063/1.4971271]

Four-wave mixing (FWM) is a decisive technique that has been widely used in wavelength-division multiplexing systems, in particular for wavelength conversion, negative frequency chirping and fiber wavelength dispersion compensation.[1,2] With the recent emergence of commercial coherent systems, FWM can also be envisioned to develop novel types of wavelength converters for any advanced modulation formats,[3,4] as well as for all-optical signal processing[5] in future photonic integrated circuits (PICs).[6] Most published works have shown that FWM can be generated within different nonlinear media such as nonlinear silica and photonic crystal fibers,[7,8] silicon based micro-rings,[9–11] and semiconductor optical amplifiers (SOAs).[12,13] Although the use of highly nonlinear optical fibers allows very efficient conversion, it usually requires an interaction length of several meters and a large pump power, which are not suitable for monolithic integration. Another important issue with optical fibers is that the required fiber length combined with an operation away from the zero-dispersion wavelength strongly affects the wave mixing and can alter conversion efficiency. On the other hand, recent works have reported efficient FWM with relatively low power consumption in micro-ring resonators. However such resonators usually require 4 ports vertically coupled to low-loss bus waveguides, and fabrication costs may thus be an issue as compared to a simple SOA. In the latter, FWM is obtained from the beating between the incident pump and probe beams and phase-matching is ensured owing to the hetero-structure confinement. From a microscopic viewpoint, the wave mixing is piloted by the third-order nonlinear susceptibility $\chi^{(3)}$ through different mechanisms.[14] In the low-frequency region, the beating between the pump and probe causes carrier density pulsation (CDP) which enhances $\chi^{(3)}$, hence the static conversion, but with a slow response speed inherently limited by the carrier recombination lifetime of interband processes (sub-nanosecond timescale). In contrast, carrier heating (CH) and spectral hole burning (SHB), occurring within subpicosecond timescales, allow pushing the dynamic frequency conversion over much larger bandwidths, enabling signal conversions with faster modulation rates. Although both SHB and CH contribute to increase the bandwidth, these also reduce the amplitude of the $\chi^{(3)}$, leading to a trade-off between efficiency and bandwidth of the conversion. Finally, another detrimental effect that must be eliminated for practical applications is the asymmetry of the conversion efficiency (i.e. between up- and down-converted

[a]Electronic mail: heming.huang@telecom-paristech.fr
[b]Also with King Abdulaziz University, Jeddah 21589, KSA
[c]Also with Center for High Technology Materials, University of New-Mexico, 1313 Goddard SE, Albuquerque, NM, United States

signals), which stems from out-of-phase contributions to $\chi^{(3)}$ of the CDP, CH, and SHB.[1,15] In order to overcome these limitations, semiconductor quantum dots (QD) constitute a class of nanostructures exhibiting large optical nonlinearities and high response speeds owing to the fast carrier-carrier and carrier-phonon scatterings.[15–17] For instance, previous works have revealed that fast FWM can be obtained in QD media through deeper spectral holes originating from the fast carrier scattering rate into the depleted states.[16] However, unlike quantum well (QW) materials where the large carrier density increases the CH via free-carrier absorption, the latter is less predominant in QDs in particular for nanostructures with a large conduction-band offset. Consequently, in QD materials, the symmetry of the conversion arising from the phase difference between CDP, SHB, and CH, is mainly piloted by the two first contributions through the linewidth enhancement factor (LEF).[15] Hence, as opposed to bulk and QW materials, a quasi-symmetrical response between up- and down-converted signals can be obtained with QD materials as the reduced LEF leads to almost in-phase contributions of CDP and SHB. Experimental studies have mainly focused on QD SOAs owing to their large linear gain and long interaction lengths.[12,13,18,19] In contrast, little is known on the potential of using QD resonant oscillators based on either Fabry-Perot (FP) or distributed feedback (DFB) configurations. In particular, taking advantage of cavity resonances and reduced amplified spontaneous emission (ASE) noise, resonant oscillators can constitute an alternative that can produce highly non-degenerate FWM with improved amplitude and bandwidth, and with more compact dimensions. For instance, in DFB lasers where the Bragg mode is directly used as the pump, prior articles have reported efficient frequency conversions for both QW and QD active materials.[20–22] However, one of the major drawbacks in using DFBs is that complex DFB features difficult to control from device to device without careful design and processing optimizations, such as facet phase effects or grating coupling coefficient, can strongly deteriorate the conversion efficiency.[23] In this work, we present an experimental study of non-degenerate FWM in InAs/GaAs QD-based light-emitters. In order to further compress the ASE and overcome bandwidth limitations stemming from the lasers relaxation oscillation frequency (ROF), the lasers under study are also optically injection-locked.[24] Under proper injection conditions, the beating between the injected light frequency and the cavity resonant frequency dominates the dynamic behavior and enhances a carrier modulation resonance at frequencies higher than the ROF. Consequently, injection-locking can allow faster modulation of the converted signals as already reported for InGaAs/InP DFB QW lasers[25] and was recently used with InAs/InP FP lasers both made with different types of nanomaterials.[26,27] Conversion efficiencies as high as -16 dB and large optical signal-to-noise ratios (OSNR) of 36 dB are reported. Quasi-symmetrical responses of the up- and down-conversion efficiency are unveiled with conversion bandwidths of up to 4 THz.

The two devices under study, noted L_1 and L_2, respectively, are InAs/GaAs QD FP lasers having the same active region. The active region is a dots-in-a-well structure incorporating 10 InAs QD layers grown by molecular beam epitaxy (MBE) and embedded in InGaAs QWs.[28] The dimensions of the nanostructures are typically within 15 to 20 nm in diameter and 3 to 5 nm in height. The dot density is estimated to be of 3 to 5×10^{10} cm^{-2}. An inhomogeneous broadening of 51 meV for the

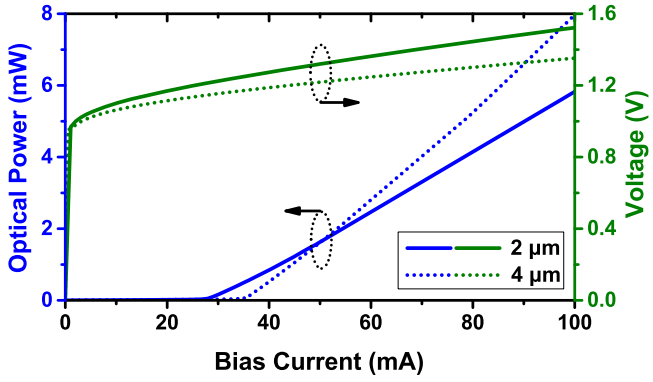

FIG. 1. LIVs measured at 2.4 $\times I_{th}$ of QD lasers L_1 and L_2.

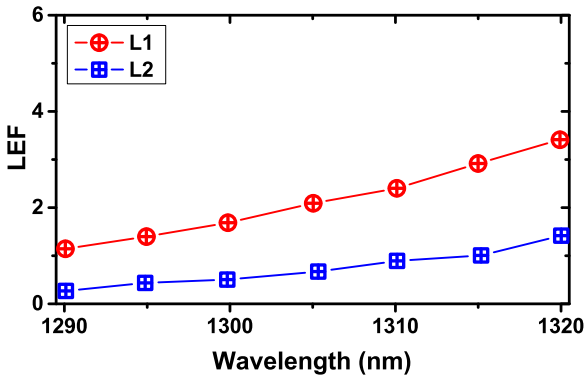

FIG. 2. Measured linewidth enhancement factor of QD lasers L_1 and L_2.

ground state transition was retrieved from photoluminescence measurements. The optical waveguide of both devices is 1.5 mm long, while the ridge waveguide (RWG) structure has a width of 2 μm for L_1 and 4 μm for L_2. The facets are left as-cleaved. All measurements were taken at 293 K. FIG. 1 presents the light-current-voltage (LIV) characteristics of both lasers. The blue lines correspond to the single facet free space output power while the green ones give the voltage across the junction. Threshold currents I_{th} of about 29 mA and 36 mA with differential quantum efficiencies of 18% and 27% are found for QD laser L_1 and L_2 respectively. The turn-on voltage is 0.95 V for both devices; the series resistance R_s is 6.3 Ω (resp. 4.3 Ω) for L_1 (resp. L_2). The center wavelengths are 1308 and 1309 nm respectively (not shown here). The below-threshold LEF is calculated by tracking the modal wavelength shift and gain change with respect to the current following the procedure described in.[26] The results are represented in FIG. 2 for both devices. At the gain peak, the LEF is about 2.5 for L_1 while it equals 0.9 for L_2.

FIG. 3 schematizes the experimental setup used. The light from two tunable lasers, TL1 and TL2, is combined by an 80/20 coupler and injected into the FP laser through an optical circulator, using a lens-ended fiber. The latter is also used to collect the light emitted by the FP. TL1 acts as master laser to lock the longitudinal FP mode at the gain peak, hence generating the pump signal for the wave mixing. TL2 is then used as probe signal. In what follows, the two QD FP lasers are biased at $2.4 \times I_{th}$, with output powers of 3.4 mW and 6.3 mW for L_1 and L_2, respectively. The power injected from TL1 is fixed 1 dB above the free-running power of the FP laser under study. The injected power from TL2 is lower in order to have little effect on the locking by TL1, and is fixed 6.3 dB below the free-running FP laser power. The FWM frequency detuning Δf, defined as the frequency difference between TL2 and TL1, is tuned to have the probe coincide with the rejected side-modes of the FP laser, where maximum conversion is obtained. The conversion efficiency being measured from optical spectra, an optical spectrum analyzer (OSA) with a 10 pm resolution is used to acquire the optical spectrum of the FP laser. The output power of the device under study is monitored with a power meter (PM) to ensure stability of the coupling.

The conversion efficiency (CE) is expressed as:

$$\eta_{CE} = \frac{P_{conv}}{P_{probe}} \tag{1}$$

where P_{probe} is the input probe power injected into the laser, and P_{conv} the optical power of the converted signal measured from the optical spectra. The application of this definition in the case of

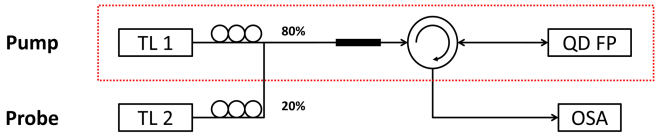

FIG. 3. Experimental setup based on optical injection configuration.

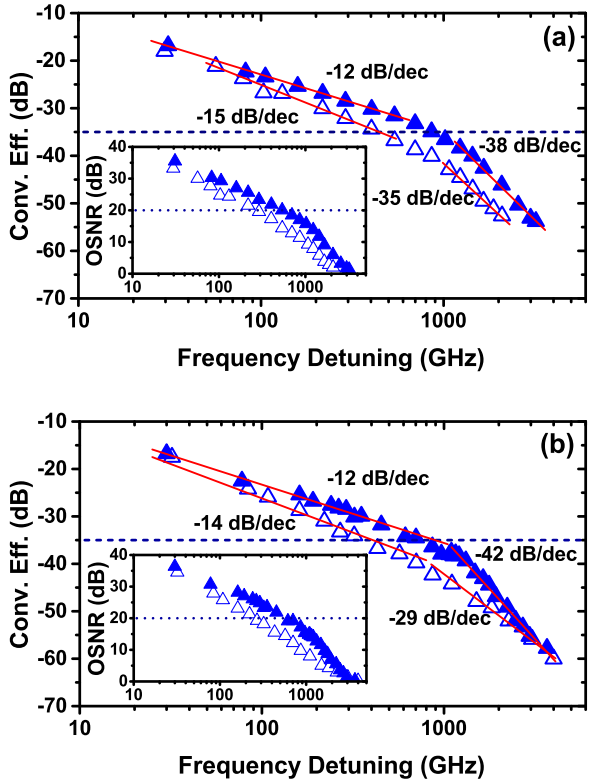

FIG. 4. Measured CE as a function of the pump-probe frequency detuning for QD lasers (a) L_1 and (b) L_2 under $2.4 \times I_{th}$ and 1 dB pump injection strength. Filled (resp. empty) triangles represent up (resp. down) conversion. The figures in inset show the corresponding OSNR of QD lasers L_1 and L_2.

a FP laser is discussed towards the end of this section. The OSNR is defined as the ratio of the peak powers of the converted signal and the highest neighboring mode of the FP cavity. FIG. 4(a) depicts the measured CE and OSNR for QD laser L_1 as a function of the absolute value of the detuning Δf. Each point on the CE profile corresponds to injection into one of the cavity modes, which is where maximal conversion can be obtained. The wavelength detunings at which the CE was measured are thus multiples of the free spectral range of the injected laser, and correspond to local maxima in the curve of the CE as a function of the pump-probe detuning. In FIG. 4(a), two regions can be distinguished for both the up- and down-conversion measurements. For detunings below 1 THz, a decrease of the CE by -15 dB/decade for down-conversion and of -12 dB/decade for up-conversion is piloted by the CDP, CH, and SHB. It is then followed by a faster decrease by -35 dB/decade for down-conversion and -38 dB/decade for up-conversion, where SHB is the dominant process with sub-picosecond timescales. Due to the rather low asymmetry in the gain profile translating into a small LEF, the up- and down-conversion profiles are found to be rather symmetric as the dominant processes, i.e. the CDP and SHB, are almost in phase and interfere constructively. This direction-independence of the conversion also proves that the lasing wavelength is relatively close to the resonant dot population within the inhomogeneous broadening, given that little carrier-induced change in refractive index is expected near the resonance. Conversion efficiencies of -16 dB are observed when injecting into the first longitudinal modes around the pump signal, for $\Delta f < 100$ GHz. The CE is then always maintained above -35 dB for down-conversion within frequency detunings up to 400 GHz, and up to 900 GHz for up-conversion. For $\Delta f > 1$ THz the SHB dominates, and while the interaction is weaker the conversion expands over a large bandwidth of up to 2.1 THz for down-conversion and 3.2 THz for up-conversion. Results show that the InAs/GaAs QDs used in this work have an appropriate dephasing rate allowing a fast response without a dramatic reduction of the amplitude of the conversion. In addition, the OSNR measurements shown in the inset of

FIG. 4(a) proves that spontaneous emission, which is further compressed under optical injection-locking, allows maintaining signal-to-noise ratios above 20 dB over a wide bandwidth. Let us stress that a minimum of pump power is needed to injection-lock the laser, and optima of both the amplitude and the bandwidth of the conversion were obtained with a 1-dB injection strength. Further increase of the pump power induces a slight decrease of the CE (not shown here) of about 4 dB at 30 GHz and 2 dB at 1 THz that can be attributed to reduction of the gain with optical injection.[29] FIG. 4(b) presents the CE and OSNR measured with QD laser L_2. The behavior below 1 THz is very similar to that of L_1, with a maximum CE of -16 dB and similar slopes for both up- and down-conversion. Above 1 THz, the slopes of up- and down-conversion differ from those measured for L_1, and wavelength conversion above 3 THz is now observed for both up- and down-conversion.

Finally, the inset of FIG. 4 (b) depicts an OSNR ranging from 40 dB to 0 dB, similar to the one obtained with L_1. The enhanced bandwidth of conversion can be attributed to the wider RWG, which enhances optical linearities owing to a stronger interaction cross-section associated to the effective mode area. Fig. 4 (b) shows that the up- and down-conversion profiles are found to be more symmetrical than for L_1. Such symmetrical responses are consistent with the very low LEF measured on L_2. Let us note that, owing to the large number of QD stacks and the high concentration of nanostructures in the active region of L_1 and L_2, a high bandwidth is reached with a rather large efficiency. It is interesting to note that for the same active material, the value of the CE can be strongly increased with simple changes of the cavity mirrors. In a FP cavity, only two thirds of the injected light enters the cavity and the output power of the laser is shared between the two facets, which is not taken into account in the definition of the CE. Using a DFB cavity with anti-reflection coating on the facet used for optical injection, the latter will present low insertion losses and the CE will thus increase. Finally, comparing the results with SOAs of similar active regions, we found that the optical injection configuration allows reaching larger conversion bandwidths with lower bias currents and shorter interaction lengths.[12]

This work reports on efficient wavelength conversion in optically injected-locked FP InAs/GaAs QD lasers. Results unveil a maximum conversion efficiency of -16 dB, bandwidths up to 4 THz as well as a quasi-symmetrical response between up- and down-conversions. Optical injection if not only used to select a single mode as pump wave, but also allows using the resonance of the cavity by preventing stimulated emission in other modes and to compress their spontaneous emission. As for the active region, the discrete energy levels of the QDs concentrate the oscillator strength essentially at the resonant wavelength, leading to a reduced LEF and hence a rather symmetrical conversion. Then, the large number of QD stacks with relatively high dot density leads to an enhanced nonlinear susceptibility. The analysis of two different design geometries shows that proper RWG structure is required to maximize wavelength conversion. Finally, compared to SOAs, carefully-designed optically injection-locked QD lasers may allow reaching similar conversion performance with a lower power requirement. Since these QD-based emitters operate at 1.3 μm, i.e. around wavelengths longer than the bandgap of silicon, this work is of primary importance for wavelength conversion and optical signal processing in future silicon PICs.

This work is supported by the Institut Mines Télécom (IMT) through the Futurs & Ruptures program, by the European Office of Aerospace Research and Development under Grant FA9550-15-1-0104 and by the DFG in the framework of the SFB787. The authors acknowledge Yenista Optics for providing the external tunable laser and helping us to complete this work.

[1] C. H. Lee, *Microwave Photonics*, Second Edition (Taylor & Francis, 2013).
[2] C. W. Chow and Y. Liu, *Adv. Lasers Electro Opt.*, InTech (2010).
[3] Y. Long, J. Liu, X. Hu, A. Wang, L. Zhou, K. Zou, Y. Zhu, F. Zhang, and J. Wang, Opt. Lett. **40**, 5475 (2015).
[4] H. N. Tan, T. Inoue, and S. Namiki, IEEE Eur. Conf. Opt. Commun., 1-3 (2015).
[5] K. Weich, J. Hrer, and E. Patzak, Electron. Lett. **30**, 493 (1994).
[6] L. Vivien and L. Pavesi, *Handbook of Silicon Photonics* (CRC Press, 2016).
[7] J. H. Lee, W. Belardi, K. Furusawa, P. Petropoulos, Z. Yusoff, T. M. Monro, and D. J. Richardson, IEEE Photon. Technol. Lett. **15**, 440 (2003).
[8] T. H. Tuan, T. Cheng, K. Asano, Z. Duan, W. Gao, D. Deng, T. Suzuki, and Y. Ohishi, Opt. Express **17**, 20303 (2013).
[9] M. Ferrera, L. Razzari, D. Duchsen, R. Morandotti, Z. Yang, M. Liscidini, J. E. Sipe, S. Chu, B. E. Little, and D. J. Moss, Nat. Photon. **2**, 737 (2008).
[10] M. Ferrera, D. Duchesne, L. Razzari, M. Peccianti, R. Morandotti, P. Cheben, S. Janz, D. X. Xu, B. E. Little, S. Chu, and D. J. Moss, Opt. Express **17**, 14098 (2009).

[11] J. R. Ong, R. Kumar, R. Aguinaldo, and S. Mookherjea, IEEE Photon. Technol. Lett. **25**, 1699 (2013).
[12] C. Meuer, C. Schmidt-Langhorst, H. Schmeckebier, G. Fiol, D. Arsenijević, C. Schubert, and D. Bimberg, Opt. Express **19**, 3788 (2011).
[13] G. Contestabile, A. Maruta, and K. I. Kitayama, IEEE J. Quantum Electron. **50**, 379 (2014).
[14] H. Soto and D. Erasme, Appl. Phys. Lett. **68**, 3698 (1996).
[15] T. Akiyama, H. Kuwatsuka, N. Hatori, Y. Nakata, H. Ebe, and M. Sugawara, IEEE Photonics Technol. Lett. **14**, 1139 (2002).
[16] D. Nielsen and S. L. Chuang, Phys. Rev. B **81**, 035305 (2010).
[17] P. Borri, S. Schneider, W. Langbein, and D. Bimberg, J. Opt. A Pure Appl. Opt. **8**, S33 (2006).
[18] T. Akiyama, O. Wada, H. Kuwatsuka, T. Simoyama, Y. Nakata, K. Mukai, M. Sugawara, and H. Ishikawa, Appl. Phys. Lett. **77**, 1753 (2000).
[19] Z. G. Lu, J. R. Liu, S. Raymond, P. J. Poole, P. J. Barrios, D. Poitras, F. G. Sun, G. Pakulski, P. J. Bock, and T. Hall, Electron. Lett. **42**, 1112 (2006).
[20] A. Mecozzi and R. Hui, IEEE J. Quantum Electron. **29**, 1477 (1993).
[21] T. Simoyama, H. Kuwatsuka, and H. Ishikawa, Fujitsu Sci. Tech. J. **34**, 235 (1998).
[22] H. Su, H. Li, L. Zhang, Z. Zou, A. L. Gray, R. Wang, P. M. Varangis, and L. F. Lester, IEEE Photon. Technol. Lett. **17**, 1686 (2005).
[23] F. Grillot, IEEE J. Quantum Electron. **45**, 720 (2009).
[24] L. Li and K. Petermann, IEEE J. Quantum Electron. **30**, 43 (1994).
[25] S. Murata, A. Tomita, J. Shimizu, M. Kitamura, and A. Suzuki, Appl. Phys. Lett. **58**, 1458 (1991).
[26] H. Huang, K. Schires, P. J. Poole, and F. Grillot, Appl. Phys. Lett. **106**, 143501 (2015).
[27] T. Sadeev, H. Huang, D. Arsenijević, K. Schires, F. Grillot, and D. Bimberg, Appl. Phys. Lett. **107**, 191111 (2015).
[28] A. R. Kovsh, N. A. Maleev, A. E. Zhukov, S. S. Mikhrin, A. P. Vasil'ev, E. A. Semenova, Yu.M. Shernyakov, M. V. Maximov, D. A. Livshits, V. M. Ustinov, N. N. Ledentsov, D. Bimberg, and Z. I. Alferov, J. Cryst. Growth **251**, 729 (2003).
[29] M. Gioaninni, A. Sevega, and I. Montrosset, Opt. Quant. Electron. **38**, 381 (2006).